Numerical and Experimental analysis of a Solar Air Heater with triangular ducts

Rambabu Dara
Department of Mechanical Engineering,
Indian Institute of Information Technology Design and Manufacturing Kurnool
Kurnool, Andhra Pradesh, India

Pullarao Muvvala
Department of Mechanical Engineering,
Indian Institute of Information Technology Design and Manufacturing Kurnool
Kurnool, Andhra Pradesh, India

Hasan Baig*
Department of Engineering & Construction
School of Architecture, Computing and Engineering
University of East London, London, UK
e–mail: H.baig@uel.ac.uk

ABSTRACT

The solar air heater is a device that uses the freely available solar energy and converts it to thermal energy using a working fluid like air. These systems can be used in buildings to supplement traditional heating systems and help us reduce energy costs. The shape of the solar air heater cavity can vary depending on the design and purpose of the heater. Some common shapes include rectangular, triangular, circular, semi-circular, etc. The choice of shape can affect the efficiency of the heater and may depend on factors such as available space, desired airflow, and aesthetic considerations. This paper reports the results of a numerical and experimental investigation carried out on the isosceles triangular duct solar air heater (SAH). The parameter varied in the study is the interior angle (θ) of the isosceles triangular duct from 40º to 80º, with an interval of 5° variation. The top absorber plate width (W) is fixed at 160 mm for all duct variants. The height (H) of the duct will vary according to the duct interior angle. The influence of duct interior angle on the heat transfer performance, the bulk temperature of the air, and pressure drop across the solar air heater duct are investigated. The top surface of the duct replicates the absorber plate of the SAH and is subjected to a uniform and constant heat flux value of 1000 W/m^2. This investigation comprises of both experiments and computational simulations. The numerical problem is modelled and simulated using the commercially available ANSYS Fluent software. The two-equation standard k-epsilon model is engaged to handle the turbulence closure.

KEYWORDS

Solar air heater, triangular duct, solar energy, CFD, Thermal energy, solar energy

* Corresponding author

INTRODUCTION

Solar air heaters (SAH) are devices that utilize sunlight to heat air for residential, commercial, or industrial purposes. These systems typically consist of a solar collector, which absorbs sunlight and transfers its energy to the passing air, and a fan or blower that circulates the heated air to indoor spaces or other applications. Solar air heaters are environmentally friendly and energy-efficient, helping to reduce heating costs and carbon emissions. They can be integrated into existing HVAC systems or used as standalone units. By harnessing solar energy, these heaters provide a sustainable alternative to conventional heating methods, contributing to a greener and more sustainable future.

A solar air heater cavity refers to the enclosed space within a solar air heater system where the air is heated by absorbing solar energy. This cavity is often designed with specific materials and configurations to maximize the heat transfer from sunlight to the air passing through it. The cavity typically contains a solar absorber, which is a material that absorbs sunlight and converts it into heat. The absorbed heat is then transferred to the air flowing through the cavity, which is usually facilitated by a fan or natural convection. Proper insulation and design considerations are essential to ensure efficient heat collection and distribution within the solar air heater cavity.

The shape of the Solar air heater cavity can vary depending on the design and purpose of the heater. Some common shapes include rectangular [1], triangular [2], circular [3], trapezoidal [4], etc. The choice of shape can affect the efficiency of the heater and may depend on factors such as available space, desired airflow, and aesthetic considerations. Figure 1 shows the different duct geometries in SAH design.

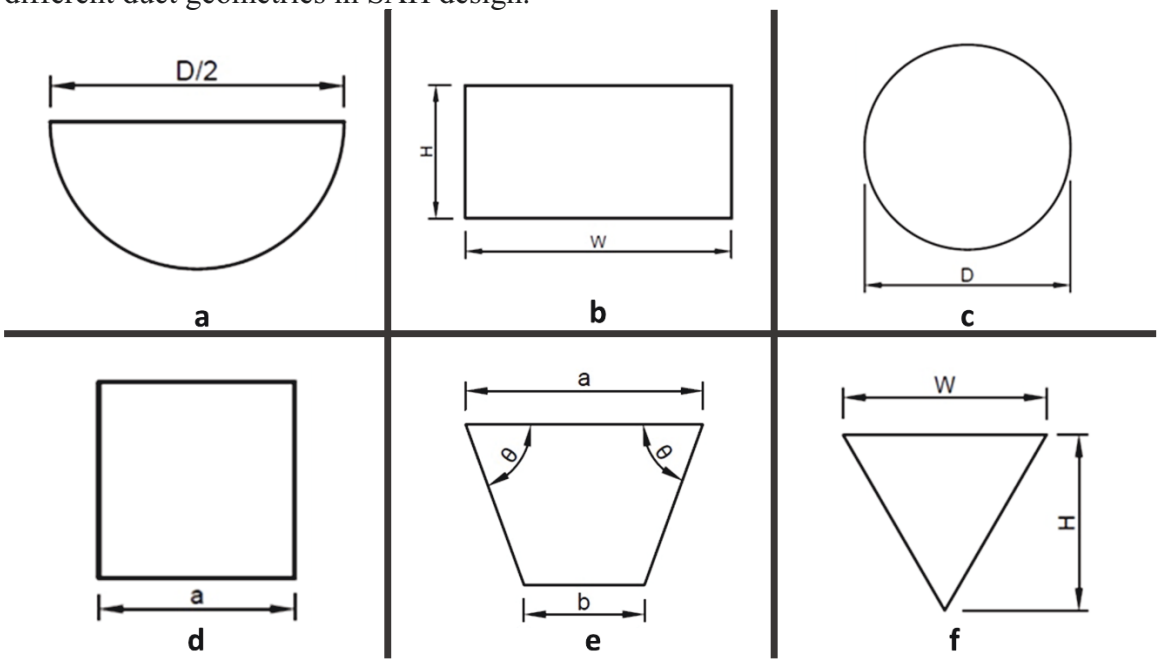

Figure 1 Different types of duct geometries in SAH: (a) Rectangular, (b) Triangular, (c) Circular, (d) Trapezoidal, (e) Square, (f) Semi-circular.

Solar air heaters can be used in buildings to supplement traditional heating systems and reduce energy costs. The SAH is a device that makes use of solar insolation, which comes from the sun and strikes the absorber plates. This absorbed solar energy will be converted into the heat energy of the working fluid, i.e., air. The heated air can be circulated through the building using a fan or natural convection. There are different types of solar air heaters, including unglazed and glazed collectors, and they can be installed on the roof, walls, or in a separate free-standing

unit. The size and number of solar air heaters needed will depend on factors such as the size of the building, the climate, and energy requirements. Solar air heaters can be a cost-effective and environmentally friendly way to provide heating in buildings, especially in sunny regions. However, their effectiveness may be limited in colder or cloudier climates, and they may need to be supplemented with other heating sources [5].

A triangular duct SAH is a type of solar air heater that has a triangular shape as shown in Figure 2. This shape is often chosen because when compared to the other geometries of the duct, the triangular solar air heater duct performs better in certain conditions, such as when the intensity of radiation from the sun is low.

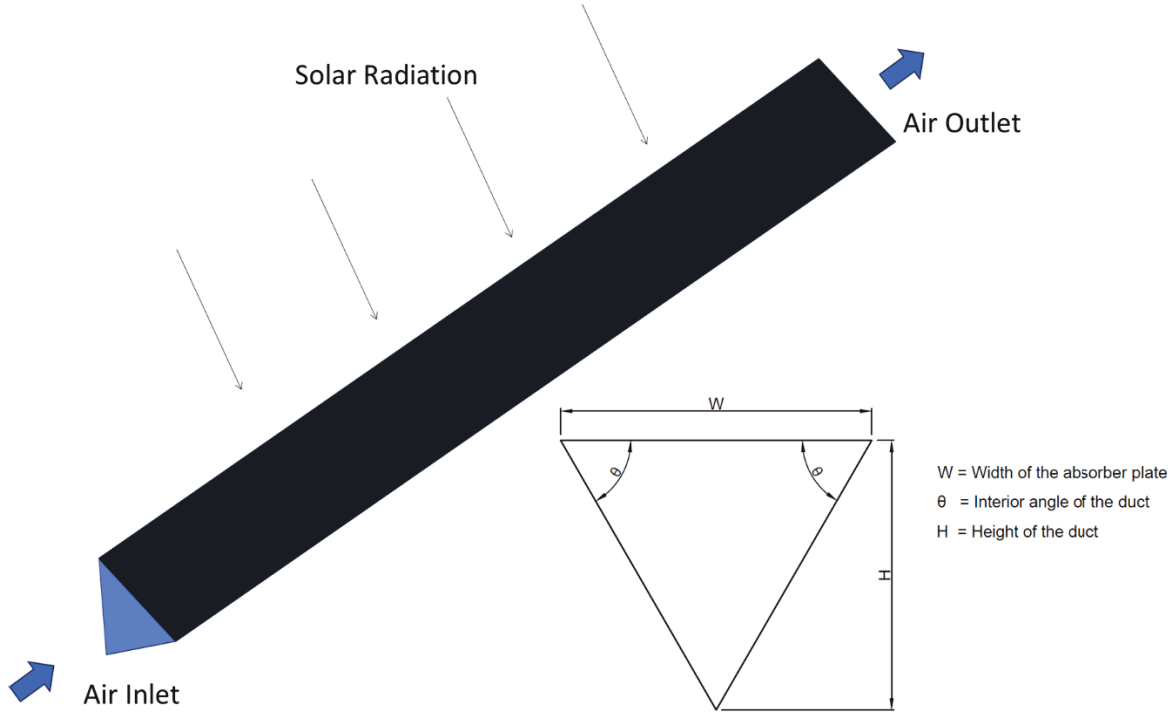

Figure 2 A triangular solar air heater duct

The triangular air heater typically consists of a dark-coloured, heat-absorbing surface that is positioned at an angle facing the sun. Air is then drawn in through an opening on one onside of the duct and gets heated by the absorber plate (which is heated by the sun) and leaves the duct at a higher temperature. The heated air can then be used to supplement traditional heating systems or to provide ventilation. The objective of the current work is to comprehensively investigate the performance of a solar air heater of isosceles triangular duct by varying the geometrical parameter of the duct, i.e. the interior angle (θ).

LITERATURE REVIEW

In recent years, different designs of solar air heaters have been used, such as booster reflectors [6], jet impingement [7], baffles, glazed and corrugated [8], heat storage material, and PCM [9]. To enhance the efficiency, different shapes of roughness geometries are incorporated, such as C-shaped [10], rectangular [11], circular [12], etc.

Behura et al. [13] conducted experiments on a rectangular duct SAH with the three sides roughened, over a Reynolds number ranging from 4,000 to 20,000. The results show that the three

sides roughened SAH efficiency is significantly larger when compared to that of the one-side roughened SAH. Kumar et al. [14] examined attributes corresponding to heat transfer and the nature of fluid flow characteristics of a triangular passage with different configurations. The results concluded that the duct model with one rounded apex, with an augmentation of ribs along the absorber plate, has a substantial effect on the improvement of heat transfer.

Gaurav Bharadwaj et al. [15] conducted experiments on ribbed triangular SAH over the Re range from 4,500 to 28,000 by varying the relative pitch roughness and height (P/e and e/D) and attack angle (α). They concluded that the greatest Nu and f are accomplished at P/e, e/D, and α values of 12, 0.043, and 60˚, respectively. Lei Wang and Bengt Sunden [16] conducted tests on the square duct to explore the local heat transfer with various roughened shape ribs for an extent of Re from 8000 to 20000. The result shows that the trapezoidal roughened shape ribs with diminishing altitude in flow direction will give the maximum Nu and f. Dara and Muvvala [17] have done a numerical analysis of the isosceles trapezoidal duct by varying the base angle of the SAH. The base angle of the duct is varied from 45 to 90° by considering six different models of SAH ducts. The results show that the enhancement in Nu and f is observed by increasing the base angle of the duct. The enhancement in Nu and f is about 20.14 and 8.21 % for the duct with the base angle of 90° at a Reynolds number value of 5000.

In this present work, an model has been built to optimize the performances such as: air bulk temperature, Nusselt number, and friction factors across the triangular duct SAH by varying the interior angle (θ) of the triangular cross-section. By varying the θ of the triangular duct (from 40° to 80° in intervals of 5°), nine different configurations of triangular-shaped ducts are obtained, and investigations are carried out on them. The width of the absorber plate of the triangular duct (W) is taken as 0.16 m, which is maintained the same for all the configurations of the ducts. The schematic diagram of the cross-section of the simple triangular duct is shown in Figure 2.

EXPERIMENTAL FACILITY

In the present investigation, the interior angle of the triangular duct is varied from 40 to 80°, and a total of nine duct configurations are obtained. However, due to the limitations, the design and fabrication of the experimental setup of a triangular duct is done with an interior angle θ = 60° and the top plate is subjected to heating. The experimental results of this design of the triangular duct are used to validate the numerical simulations. The photographic view of the experimental setup is shown in Figure 3. The SAH duct portion consists of three sub-sections, namely the entrance, test, and exit sections, with lengths taken as per Table 1.

Table 1. Details of the operating/geometric parameters

Parameters	Values/Range
Overall length of duct (l)	2 m
Entrance section (l_1)	0.6 m
Test section, (l_2)	01 m
Exit section (l_3)	0.4 m
Width of the duct (w)	0.16 m
Interior angle (θ) of the duct	40° to 80°
Reynolds number (re)	5,000 to 28000
Constant heat flux (source of heat: q')	1000 W/m^2

Due attention was given to ASHRAE [18] standards while choosing the length of the entry section and exit section so that it guarantees that the flow develops fully turbulent before it reaches the test section. The centrifugal blower sucks the working fluid at ambient conditions, and the flow through the duct is regulated by a control drive. The velocity of the air is measured with the help of a pitot tube, which is connected to a single-channel electronic manometer. A heated aluminium plate replicates the absorber plate for solar incident radiation. This aluminium plate is subjected to a constant heat flux with an electrical heater (mica heater). The electrical supply to the mica heater is regulated with a DC power supply. Nineteen K-type pre-calibrated thermocouples measure the absorber plate surface temperatures at various positions. Thermocouple positions on the heater plate are shown in Figure 4. All thermocouples are connected to the data acquisition system to read the temperature data after reaching a steady state.

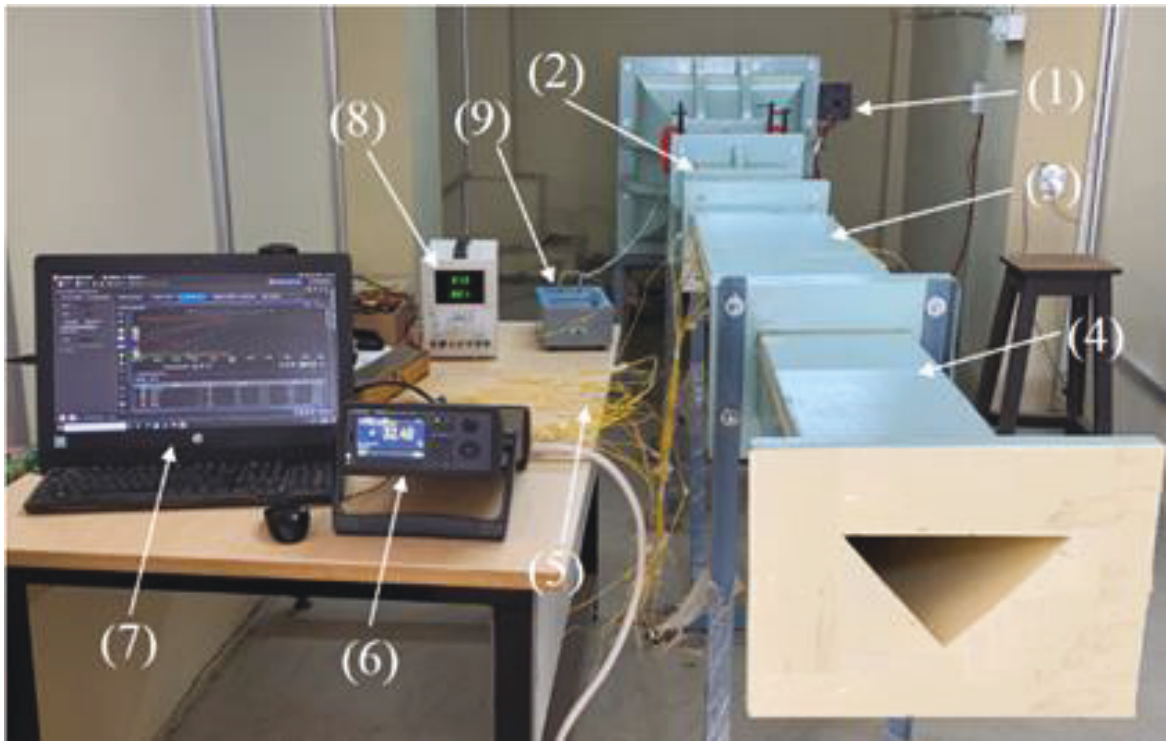

Figure 3 Photographic view of the experimental setup 1. Control drive 2. Flow entrance section 3. Test section 4. Exit section 5. K-type thermocouples 6. Temperature data acquisition system, 7. Computer, 8. DC power supply, 9. Single-channel electronic manometer.

The centrifugal blower sucks the working fluid at ambient conditions, and the flow through the duct is regulated by a control drive. The velocity of the air is measured with the help of a pitot tube, which is connected to a single-channel electronic manometer. A heated aluminium plate replicates the absorber plate for solar incident radiation.

This aluminium plate is subjected to a constant heat flux with an electrical heater (mica heater). The electrical supply to the mica heater is regulated with a DC power supply. Nineteen K-type pre-calibrated thermocouples measure the absorber plate surface temperatures at various positions. Thermocouple positions on the heater plate are shown in Figure 4. All thermocouples are connected to the data acquisition system to read the temperature data after reaching a steady state.

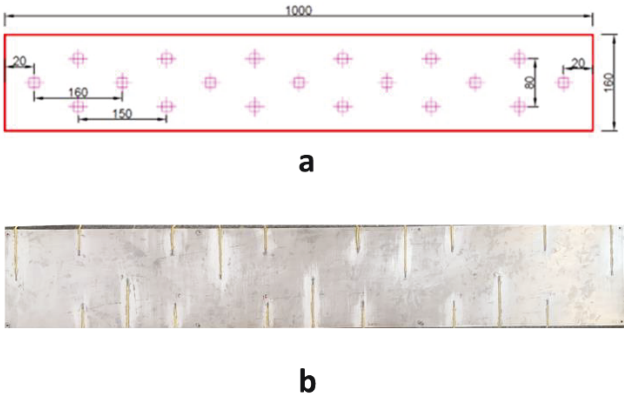

Figure 4 Thermocouple positions on the heater plate (a) Schematic view (b) Photographic view

NUMERICAL MODEL

The 3D model of triangular duct SAH is modelled and analysed by using the commercially available ANSYS Fluent software. The schematic of the SAH duct is presented in Figure 5. The overall length of the duct is 2 m. The top surface of the duct replicates the absorber plate of SAH and is subjected to a constant and uniform heat flux value of 1000 W/m^2. The CFD analysis of the triangular duct was executed over the Reynolds number (Turbulent – Condition) ranging from 5,000 to 28,000. The inlet air was considered at ambient conditions (300 K and 100 kPa). The working and geometric specifications are given in Table.1.

The problem is simulated under the following assumptions:

- The fluid flow is steady and turbulent.
- Fluid is incompressible.
- No-slip conditions at the interface of fluid and solid.
- The properties of the working fluid, i.e., air, are consistent throughout the duct, and those values are considered at ambient conditions.

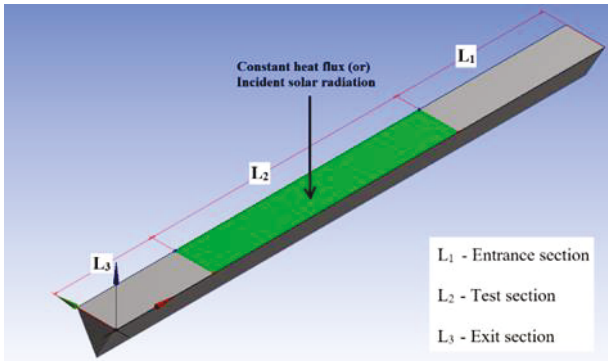

Figure 5 Schematic representation of the 3-D model of the triangular duct

Governing Equations

The fluid flow and heat transfer characteristics are achieved by solving the basic governing equations, i.e., Continuity, Momentum, and Energy Equations, coupled with the suitable turbulent closure models. In our present study, the two-equation RNG k-epsilon model (Turbulence) is used; the term k speaks to the kinetic energy of turbulence, and ε speaks to the rate of turbulence dissemination.

Boundary Conditions

The problem domain comprises of the boundaries, namely: the inlet, outlet, heated plate, and adiabatic wall. The boundary of the inlet is considered as the velocity inlet which relies on the Reynolds number value. The boundary of the outlet is considered a pressure outlet with a value of zero-gauge pressure. Finally, the heated plate is considered as conducting material and all other walls are considered as non-conducting material. A stable enduring heat flux (q′) of 1000 W/m2 is applied to the heated plate. At the solid and fluid interface, non-slip conditions are considered. The turbulence intensity of the turbulent flow can be evaluated by the following equation (1).

$$I = \frac{0.16}{(Re)^{1/8}} \qquad (1)$$

Solution Strategy

To predict the Nu_{avg}, bulk temperature of air, and f_{avg}, the solution domain is divided into a small number of grid points, and at each grid point, the governing equations are solved. The equations are discretized by utilizing the segregated grid method and second-order upwind scheme. The equations are solved until they achieve the given convergence criteria. The pressure-linked equations are worked out by using the Semi-Implicit method.

Grid Independence Test

In the present study, the number of grid elements varied from 105678 to 791721. The points of interest of the grid independence study are shown in Table 2.

Table 2: Mesh-Convergence test for Nusselt number

S.No	Total Elements	Nu	% Error in Nu
1	105678	82.65	Nil
2	161397	83.40	0.92
3	318816	83.94	0.64
4	487872	84.06	0.14
5	791721	84.14	0.10

From this, it is observed that more than the grid elements of 487872, the variation in the Nusselt number is around 0.1% only. Hence, this grid pattern with 487872 elements is considered for all the simulation purposes.

Due to the turbulent flow condition, the viscous sublayer's development occurs under the SAH's walls. Special attention was given to the solid and fluid interface during the mesh generation. The distance between the walls to the first cells is maintained within the range of 1 to 5. The parameter which predicts the distance between the walls to the first cell is represented by y+, and it is given by Equation (2).

$$y^+ = \frac{\rho U_t \Delta y}{\mu} \quad (2)$$

RESULTS AND DISCUSSION

The outcomes of this analysis such as the coefficient of heat transfer (h), and pressure drop (Δp) throughout the SAH duct section are taken into consideration for calculating the average Nu and average f across the test zone. The inlet velocity of the flow is calculated based on the Re. The equations are expressed as

Hydraulic diameter of the duct:

$$D_h = \frac{4A}{P} \quad (3)$$

Reynolds Number

$$Re = \frac{\rho U D_h}{\mu} \quad (4)$$

Surface Average Nusselt Number

$$Nu = \frac{hD_h}{K_{air}} \quad (5)$$

Average friction factor

$$f = \frac{1}{2\rho U^2} D_h \frac{\Delta p}{L_{test}} \quad (6)$$

The bulk temperature at a particular section of the duct is calculated by taking the ratio of the rate of flow of energy to the heat capacity through the cross-section, and it is given by:

$$T_b = \frac{\iint \rho u C_p T dA}{\iint \rho u C_p dA} \quad (7)$$

The change in bulk temperature (ΔT_{inc}) of air is the difference in the working fluid temperatures at the outlet and inlet sections of the duct.

Validation of Present Simulated Results

In CFD, different types of turbulence models are available to validate the results with empirical formulas. The turbulence models are RNG k-ε, Standard k-ε, Realizable k-ε, SST k-ω, Standard k-ω, etc. The CFD results are compared with the results obtained with the standard correlations. The Dittus-Boelter and Modified Blasius equations are given by Equations 8 and 9 respectively.

$$Nu_{avg} = 0.024\, Re^{0.8} Pr^{0.4} \quad (8)$$

$$f_{avg} = 0.085 Re^{-0.25} \quad (9)$$

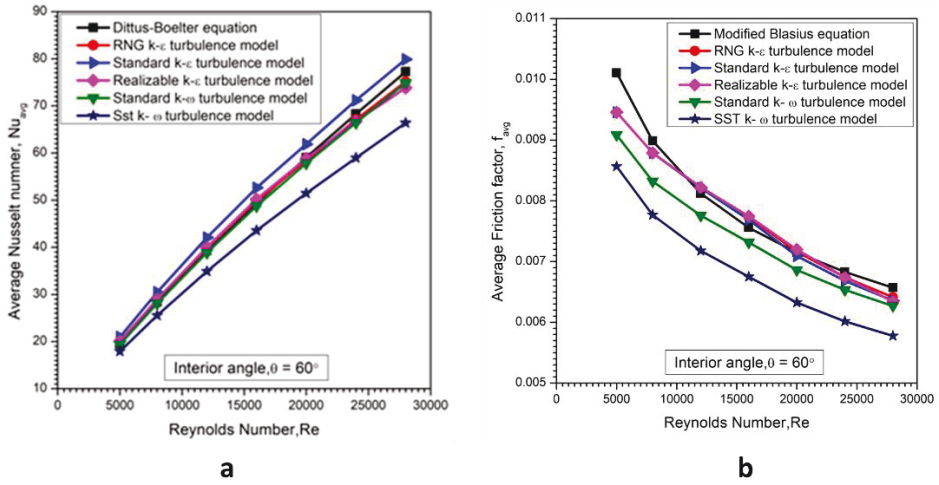

Figure 6 Validation of the Turbulence model with empirical formulas (a) Average Nusselt number (b) Average friction factor

From Figure 6, it is noticed that the RNG k-ε turbulence model shows a good match with the Dittus-Boelter equation with a maximum deviation of ±4.5 % at low Reynolds numbers. The remaining turbulence models are either under or over-predicting the results with respect to the Dittus-Boelter equation with a higher deviation. It is also observed that the RNG, Standard, and Realizable k-ε turbulence models show almost identical results with a maximum deviation of ±5.3% related to the Modified Blasius equation. By taking into the consideration of both the heat transfer and friction factors, the RNG k-ε model is used for further investigations.

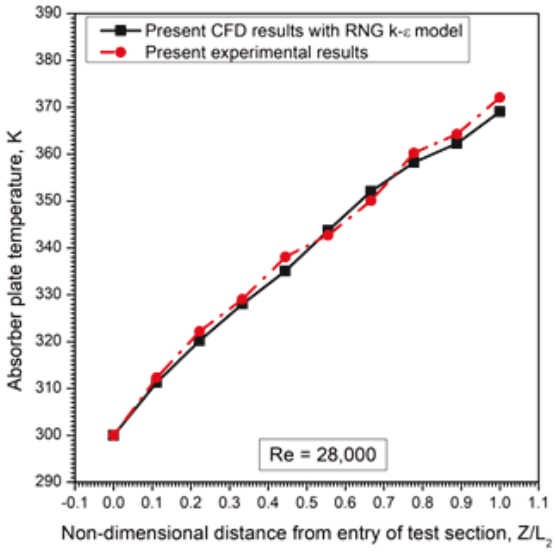

Figure 7 Validation of the present computational results with the experimental values of the local temperature on the heater surface

From Figure 7, it is seen that the local temperatures measured along the heater section in both the experimental and CFD cases (with the RNG k-ε model) are in almost good match. In this investigation, the effect of duct interior angle on the Nu_{avg}, f_{avg} and bulk temperature of air are analysed over a wide range of Reynolds numbers.

Variation of the Average Nusselt Number (Nu_{avg})

Figure 8 shows the average Nusselt number (Nuavg) variation with the interior angles (θ) of the triangular duct at various Reynolds numbers. It is noticed that at a specific Re, the average Nusselt number increases with an increase in the duct interior angle from 40˚ to 80˚. This is due to the increase in the hydraulic diameter of the duct due to an increase in the interior angle. Moreover, due to an increase in the duct angle under a particular Re value, the air velocity reduces, due to which the fluid contact time with the absorber plate increases leading to an increase in Nu value. As expected, it is also noticed that with an increment in the Re, the Nu is increasing, supporting the Dittus-Boelter equation mentioned in equation 8. At Reynolds number value of 5000, the Nusselt number value for the duct with a base angle of 80° is about 31.9% higher than that of the duct with a base angle of 40°. Whereas, at the Reynolds number value of 28000, the Nusselt number value for the duct with a base angle of 80° is about 26.7 % higher than that of the duct with a base angle of 40°. Figure 9 shows the velocity contours across the duct for the interior angles of 40° and 80°. It is clear that the velocity is very low for the duct with an interior angle of 80° as compared to the duct with an interior angle of 40°.

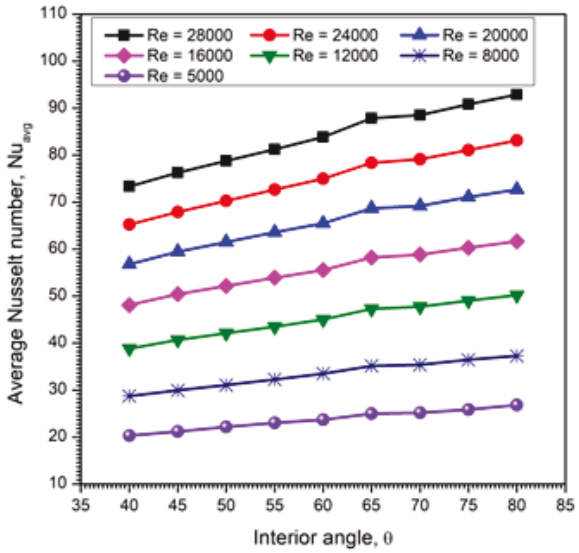

Figure 8 : Average Nusselt number variation (Nuavg) with the duct interior angles from 40˚ to 80˚

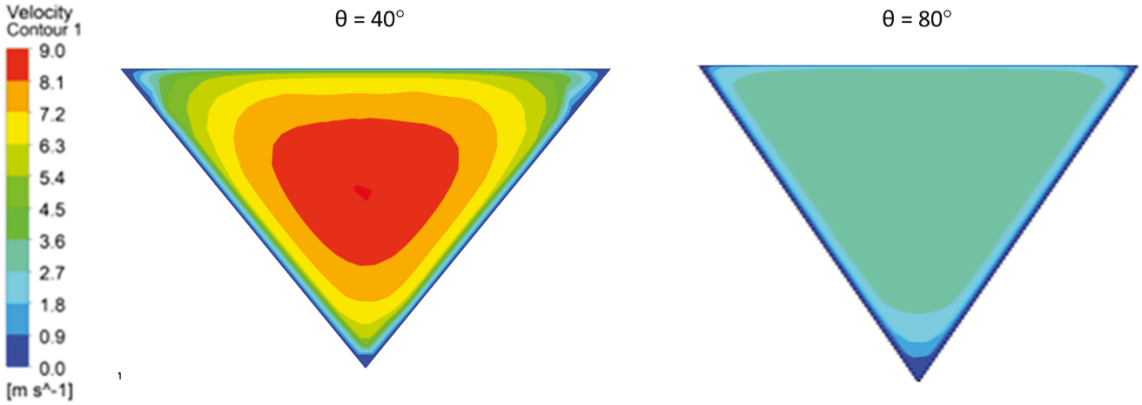

Figure 9 Velocity contours across a cross-section of the duct at Re = 28000 for interior angles of 40° and 80°

Figure 9 shows the velocity contours across the duct for the interior angles of 40° and 80°. The velocity is very low for the duct with an interior angle of 80° as compared to the duct with an interior angle of 40°.

Variation of Average Friction Factor (f_{avg})

The variation of average friction factor (f) w.r.t the duct interior angle is depicted in the Figure 10 (a) at various Reynolds numbers. At a specific Re, the average friction factor value increases with an increase in the interior angle from 40˚ to 80˚. This can be due to the increment within the hydraulic diameter of the duct and the decrease in the stream of fluid velocities. These results corroborate the friction factor equation defined in equation 6, where the friction factor is directly proportional to the hydraulic diameter of the duct and inversely proportional to the square of the fluid velocity in the duct. It is also noticed that with an increment in the Reynolds number, the friction factor decreases, supporting the Modified Blasius equation mentioned in equation 8.
At Reynolds number value of 5000, the friction factor value for the duct with an interior angle of 80° is about 22.9% higher than that of the duct with an interior angle of 40°. Whereas, at the Reynolds number value of 28000, the friction factor value for the duct with an interior angle of 80° is about 26.7% higher than that of the duct with an interior angle of 40°.

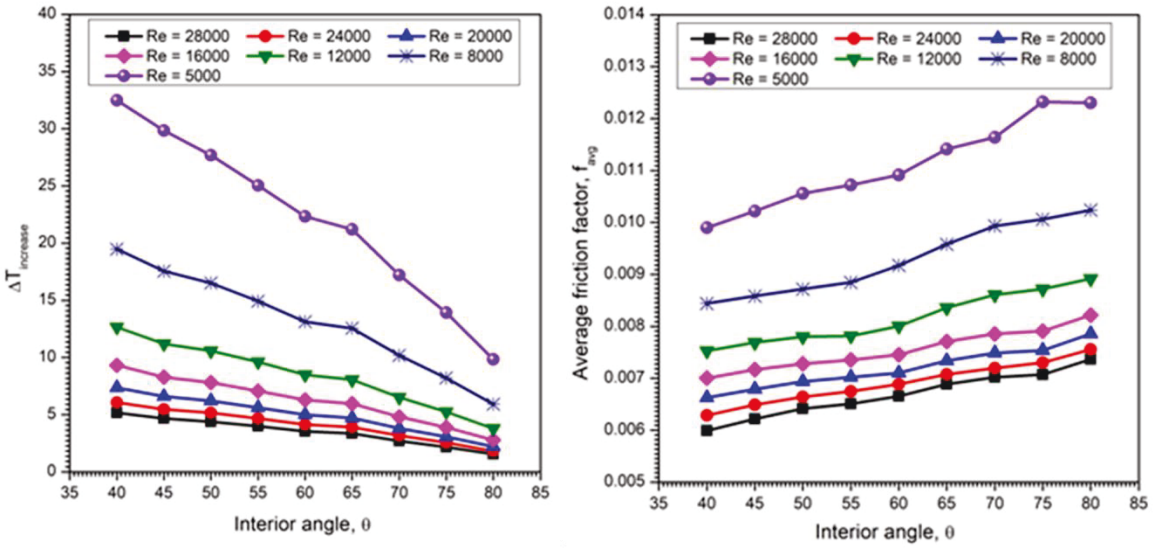

Figure 10 (a) Average friction factor (f_{avg}) variation with the interior angles from 40˚ to 80˚ (b) Bulk temperature increase (ΔT_{inc}) variation with the interior angles from 40˚ to 80˚

Figure 10 (b) shows the change in bulk temperature of air (ΔT_{inc}) along the duct with the duct interior angle (θ) of the duct, when the absorber plate is subjected to a steady heat flux condition of 1000 W/m^2 for all cases. At a particular Re, ΔT_{inc} decreases when the interior angle is increased from 40° to 80°. As all the duct variants are subjected to the same inlet conditions of air, this indicates that the bulk temperature of air at the duct outlet diminishes with an increase in the duct interior angle. At a Reynolds number value of 5,000, ΔT_{inc} decreased by about 230% from 40° to 80°. It is also observed that the maximum increase in bulk temperature (ΔT_{inc}) is seen at the lowest Reynolds number. At low Reynolds numbers, the working fluid will move at lower speeds. Due to this, there is sufficient time for the working fluid to extract higher amount of heat from the absorber plates.

Figure 11 shows the temperature contours across the duct at a Re value of 5,000 for the interior angles of 40° and 80°. It is clear that the temperature is very low for the duct with an interior angle of 80° as compared to the duct with an interior angle of 40°.

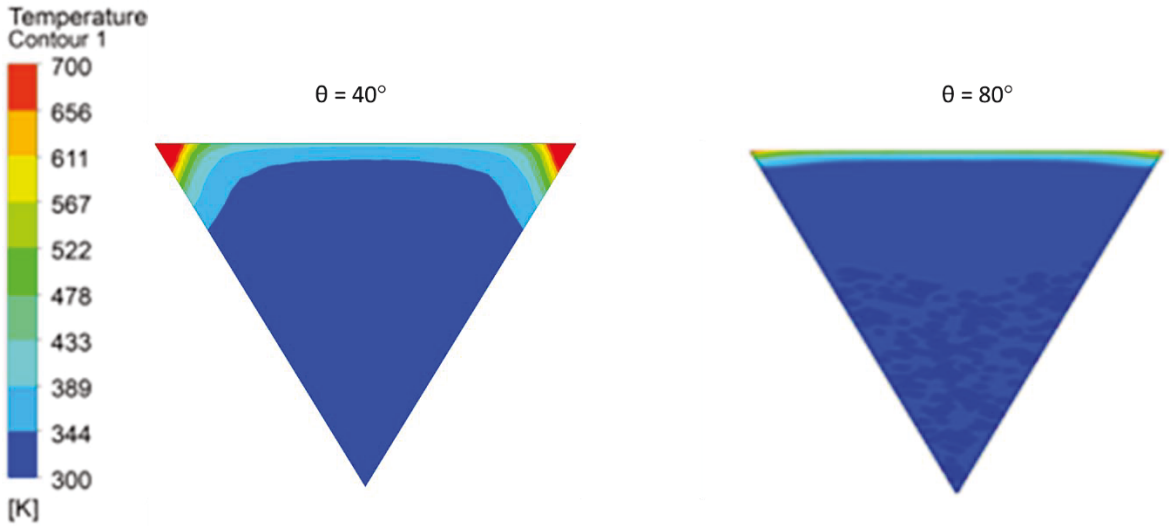

Figure 11 Temperature contours across a cross-section of the duct at Re = 5000 for interior angles of 40° and 80°

Variation of Overall Performance Factor (λ)

The Nusselt number and friction factors are two conflicting parameters of a heat exchanger's performance. Hence, the overall performance factor (λ) similar to that delineated in Manglik [19] is espoused to analyse the overall performance (combined heat transfer and friction factor performances) of heat exchangers, and it is given by Equation 10.

$$\lambda = \frac{j}{f^{1/3}} \tag{10}$$

Here, j is the Colburn j factor and is given by

$$j = St.\,\mathrm{Pr}^{2/3} \tag{11}$$

Figure 12 shows the overall performance factor variation with the interior angles of the ducts from 40˚ to 80˚. It is seen from the figure that the overall performance (λ) increases with an increasing the interior angle of the duct from 40 to 80°. At Reynolds number value of 5000, the overall performance factor value for the duct with an interior angle of 80° is about 22.72% higher than that of the duct with an interior angle of 40°. It is also observed that the λ increases with a decrease in Reynolds number.

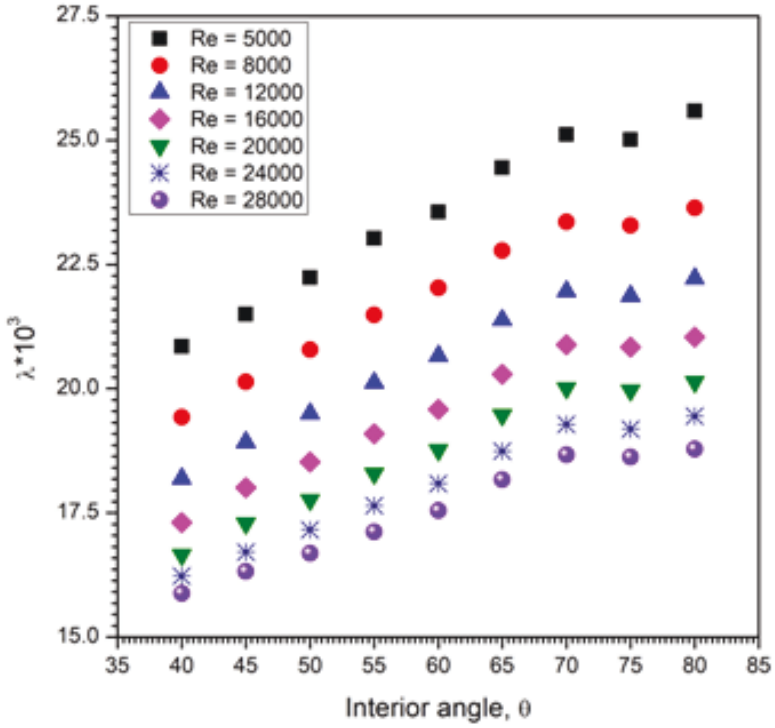

Figure 12 Variation of overall performance factor (λ) with interior angles from 40˚ to 80˚

CONCLUSIONS

In this work, nine different interior angles of the duct ranging from 40˚ to 80˚ were examined in order to determine the fluid flow and heat transfer characteristics of the air in triangular duct SAH. The below conclusions drawn from this study:

- The average Nusselt number (Nuavg) value increases with an increase in the interior angle of the triangular duct from 40˚ to 80˚. At Reynolds number value of 5000, the Nuavg value for the duct with an interior angle of 80° is about 31.9% higher than that of the duct with an interior angle of 40°.
- A similar tendency is seen for the friction factor value also. The friction factor increases with an increase in the interior angle from 40˚ to 80˚. At a Reynolds number value of 5000, the f_{avg} value for the duct with the interior angle of 80° is about 22.9 % higher than that of the duct with the interior angle of 40°.
- An overall performance factor (λ) is defined to get the combined heat transfer and friction performances. It is noticed that the triangular-shaped SAH duct with an interior angle of 80˚ is giving the best overall performance over the nine configurations of the ducts investigated in the study.
- Whereas the increment in the duct interior angle (θ) from 40˚ to 80˚ is not favourable with respect to the ΔT_{inc} leading to a decrease of nearly 230%.

The main motto of the SAH is to heat the air, i.e., to get a higher bulk temperature of the air at the duct outlet, which can be used in buildings to supplement traditional heating systems and reduce energy costs. From this detailed investigation, it is found that the triangular duct with an interior angle of 40˚ is the best configuration among all the configurations of the ducts considered in the study.

NOMENCLATURE

A_{cs}	cross-sectional area of the duct	[m^2]
C_p	specific heat	[J/kg K]
D_h	hydraulic diameter	[m]
h	convective heat transfer coefficient	[W/m^2K]
K	thermal conductivity	[W/m K]
L	overall length of duct	[m]
p	pressure	[Pa]
U	velocity	[m/s^2]
W	width of the duct	[m]
Greek Symbols		
ε	viscous dissipation rate	[m^2/s^3]
θ	interior angle of the duct	(Degrees)
μ	dynamic viscosity	[$N/m^{2]}$]
k	turbulent kinetic energy	[m^2/s^2]
λ	overall performance factor	
ρ	density of air	[kg/m^3]
ΔT_{inc}	Increase in the bulk temperature of air from the duct inlet to the outlet	[°C]

Dimensionless Numbers

f	Friction factor
I	Turbulence intensity
j	colburn j factor
Nu	Nusselt number
Re	Reynolds number

REFERENCES

1. R.P.Saini, Jitendra Verma, Heat Transfer and friction factor correlations for a duct having dimple-shape artificial roughness for solar air heaters, *Energy* Vol. 33, pp. 1277-1287, 2008.
2. Varun Goel, Pankaj Guleria, Rajneesh Kumar, Effect of apex angle variation on the thermal and hydraulic performance of rounded triangular duct, *International Communications in Heat and Mass Transfer*, Vol. 86, pp. 239-244, 2017.
3. Shetty S P, Madhwesh N, Karanth KV, Numerical analysis of a solar air heater with circular perforated absorber plate, *Solar Energy* 215: 416-433, 2021.
4. Dara R, & Muvvala P Effect of Base Angle of an Isosceles Trapezoidal Solar Air Heater Duct on Flow and Thermal Characteristics—A Numerical Investigation. *Journal of Solar Energy Engineering*, Vol 145, pp 041008, 2023.
5. O.V. Ekechukwu, Review of solar-energy drying system I: an overview of drying principles and theory, *Energy Conversion & Management,* Vol. 40, pp 593-613, 1999.
6. Ashwini Kumar, Thermal performance characteristics of three sides artificially roughened solar air heaters with and without booster mirrors, *International Research Journal of Advanced Engineering and Science*, Vol.1, pp 161-167, 2016.
7. Singh, S., Chaurasiya, S.K., Negi, B.S., Chander, S., Nemś, M. and Negi, S., Utilizing circular jet impingement to enhance thermal performance of solar air heater. *Renewable Energy*, Vol. 154, pp 1327-1345, 2020.

8. Djamel Sahel, Redouane, Thermal characteristic in solar air heater fitted with baffles and heating corrugated surface, *Energy Procedia* Vol. 139, pp. 307-314, 2017.
9. Ramin Moradi, Ali Kianifar, Somchai Wongwises, Optimization of a solar air heater with phase change materials: Experimental and numerical study, *Experimental Thermal and Fluid Science*, Vol. 89, pp 41-49, 2017.
10. Saravanan A, Murugan M, Reddy MS, Ranjit PS, Elumalai V, Kumar P, Sree SR Thermo-hydraulic performance of a solar air heater with staggered C-shape finned absorber plate. *International Journal of Thermal Sciences,* Vol. 168, pp 107068, 2021.
11. Boulemtafes-Boukadoum A, Benzaoui A, CFD based analysis of heat transfer enhancement in solar air heater provided with transverse rectangular ribs. *Energy Procedia* Vol. 50, pp 761-772, 2014.
12. Yadav AS, Bhagoria JL, A CFD (computational fluid dynamics) based heat transfer and fluid flow analysis of a solar air heater provided with circular transverse wire rib roughness on the absorber plate. *Energy*, Vol. 55: pp 1127-1142, 2013.
13. Arun Kumar Behura, Sachindra Kumar Rout, Thermal analysis of three sides artificially roughened solar air heaters, *Energy Procedia*, Vol. 109, pp. 279-285, 2017.
14. Rajneesh Kumar, Varun, Anoop Kumar, Experimental and computational fluid dynamics study on fluid flow and heat transfer in triangular passage solar air heater of different configurations, *Journal of Solar Energy Engineering*, Vol.139, pp 041013, 2017.
15. Gaurav Bharadwaj, Varun, Rajneesh Kumar and Avdhesh Sharma, Heat transfer augmentation and flow characteristics in ribbed triangular duct solar air heater: An experimental analysis, *International Journal of Green Energy*, Vol.14, pp. 587-598, 2017.
16. Lei wang, Bengt Sunden, Experimental investigation of local heat transfer in a square duct with continuous and truncated ribs, *Experimental Heat Transfer*, Vol. 18, pp 179-197, 2005.
17. Dara, R., and Muvvala, P., 2023. Effect of Base Angle of an Isosceles Trapezoidal Solar Air Heater Duct on Flow and Thermal Characteristics—A Numerical Investigation. *ASME. J. Sol. Energy Eng,* Vol. 145, pp 041008, 2023
18. ASHRAE standard, Methods of testing to determine the thermal performance of solar collectors, ANSI/ASHRAE, 93-1986. 1977.
19. Manglik, R. M., Heat Transfer Enhancement, *Heat Transfer Handbook*, pp. 1029-1130, 2003.